AutoMorFi: Automated Whole-image Morphometry in Fiji/ImageJ for Diverse Image Analysis Needs

Ouzéna Bouadi[1], Chenkai Yao[2], Jason Zeng[1], Danielle Beason[2], Nyomi Inda[3], Zoe Malone[1], Jonathan Yoshihara[1], Amritha Vinayak Manjally[1], Clifton Johnson III[1], Jonathan Cherry[4], Chin-Yi Chen[5], Tzu-Chieh Huang[5], Bogdana Popovic[5], Maria Henley[5], Guangmei Liu[1], Elizabeth Kharitonova[6], Ella Zeldich[6], Hannah Aichelman[1], Sarah W. Davies[1], Peter Walentek[7], Yuan Tian[1], Hengye Man[1], Elif Ozsen[1], Kristen Harder[1], Thomas Gilmore[1], David Pitt[5], Tuan Leng Tay[1,8*]

Affiliations:

[1]Department of Biology, Boston University, Boston, MA 02215, USA

[2]Department of Biomedical Engineering, Boston University

[3]Department of Electrical and Computer Engineering, Boston University

[4]Department of Pathology and Laboratory Medicine, Boston University School of Medicine, Boston, MA 02118, USA

[5]Yale School of Medicine, Yale University, New Haven, CT 06510, USA

[6]Department of Anatomy & Neurobiology, Boston University School of Medicine

[7]Department of Medicine IV, University Medical Center Freiburg, Freiburg, Germany

[8]Department of Anatomy and Neurobiology, Boston University School of Medicine

*Correspondence:

Tuan Leng Tay, PhD <tltay@bu.edu>

ABSTRACT

Running on the highly popular and accessible ImageJ/Fiji platform for biological image analysis, we have established AutoMorFi as a streamlined interface for automated whole-image morphometric analysis that generates at least 47 measurements per cell or object in under 1 minute. We performed multiple validated cluster analyses on nonredundant morphometric parameters derived from AutoMorFi for various cell types, objects and organisms. We used images of rodent macrophages, human postmortem brain tissues from multiple sclerosis (MS) and Alzheimer's disease (AD) patients, iPSC/animal models for Down's syndrome and autism spectrum disorder (ASD), and organisms such as sea anemone and corals. AutoMorFi's adaptability extends across diverse imaging modalities including brightfield, confocal, or widefield fluorescence microscopy as well as underwater photography. Due to its ability for unlimited and unbiased sampling across any given image and high potential for modification and customization, AutoMorFi represents a transformative tool that will accelerate morphometric analysis and offer broad relevance in biological studies.

MAIN TEXT

Morphometry is a bedrock for understanding life sciences. The study of cellular and organismic morphology has been achieved through methods ranging from meticulously hand-drawn neurons and camera lucida traces of glia[1–3] to computational and machine-learning-based image analysis tools that classify cells and animal species by their diverse characteristics[4–6]. Current semi-automatic processes for common applications such as cell detection, quantification, and morphometry are, however, mostly out of reach for many researchers who are unfamiliar with coding languages[7]. The day-to-day reality of image data analysis involves manual adjustments of brightness, contrast, and thresholds for each image as well as painstaking tracing and validation of individually segmented cells or objects. Accurate execution of these routine tasks requires varying in-depth subject knowledge and depends on the complexity and proximity of the objects of interest. Ideally, morphometric analysis tools should be user-accessible, generate accurate results that can be easily quality controlled, offer options for unbiased and batch sampling, and highly versatile and customizable to address multifaceted scientific questions.

For nearly 3 decades, ImageJ or Fiji[8,9] has been the go-to open-source platform for researchers globally to process and analyze images as well as to reconstruct cells and objects acquired by microscopy to obtain quantitative morphometric data. Taking advantage of this familiar resource,

we aimed to standardize and automate the acquisition of multiple morphological parameters of complex and branched cells such as the highly ramified brain-resident microglia during homeostasis, by looping a series of Fiji commands using a macro[10]. We invited 30 users ranging from high school interns to principal investigators to test our first prototype, "AutoGliji", on a standard fluorescence image of IBA-1-immunolabeled mouse microglial cells (**Fig. 1A**). Testers were asked to perform manual measurements of the same 3 cells using Analyze Particles and the Simple Neurite Tracer ImageJ plugin[11] for comparison (**Fig. 1A-C**). The time needed to analyze all cells in the image by AutoGliji (5.5 ± 0.75 minutes) was drastically reduced when compared to manual measurement of 3 cells (105 ± 19 minutes) (**Fig. 1D**). Furthermore, manual measurements of over half of the parameters were highly inconsistent across testers due to different levels of familiarity with microglial morphology, in stark contrast to the reproducible results from AutoGliji which were generated by the same users (**Fig. 1E-N**).

AutoMorFi is an optimized version of AutoGliji which generates 33 measurements and 14 calculated parameters per cell or object (**Table 1, Supplementary Information 1–3, Code**). AutoMorFi macro runtime was reduced to under 1 minute (**Supplementary Video 1**) and sampling limit within any 2-dimensional 8-bit TIFF image that could be opened in Fiji was eliminated. To validate our hypothesis that 47 measures are sufficient to distinguish and classify cells based on morphology, we analyzed 393 microglia, 438 cardiac macrophages, 201 alveolar macrophages, 307 liver Kupffer cells, 332 kidney macrophages, and 274 splenic macrophages from the same wildtype adult mice that were immunolabeled with IBA-1[12–14] (**Fig. 2**). As expected, microglia and cardiac macrophages are most morphologically distinct and macrophages of the kidney, liver, lung, and spleen share an intermediate phenotype (**Fig. 2F**).

To assess the potential of AutoMorFi for diagnostic and future large-scale applications, we tested its ability to cluster microglia identified by a single IBA-1 marker in well-documented lesions of MS from patients and controls (**Table 2**, **Fig. 3**). Microglia play different roles in all stages of demyelination, oligodendrocyte death, and neuroaxonal injury in MS[15–18]. While microglia exhibit degenerative and pro-inflammatory features as MS progresses, they also participate in neuroprotection and repair. Thus, exploring microglial morphological diversity in different lesions may unveil new strategies against microglia-driven neurodegeneration in MS. Cluster analysis revealed a clear transition of microglial morphology from control WM to the rim of chronic active lesions (**Fig. 3C-F**) and 11 key morphological features that promoted optimal classification of the pathological stages (**Fig. 3G-J**). AutoMorFi appears to provide a cost-effective and time-efficient

alternative as a diagnostic tool in contrast to multiple immunohistochemical assays. Furthermore, evaluation of AutoMorFi against well-established open-source segmentation tools, including CellProfiler, ilastik, Cellpose, and QuPath suggests that only AutoMorFi offers high confidence in capturing intricate characteristics of complex and densely distributed cells with the operational efficiency necessary for handling large datasets.

As further proof-of-principle, AutoMorFi was applied to diverse image types from widefield or confocal fluorescence and brightfield microscopy as well as underwater photography (**Fig. 4**). These images represent diverse applications such as the comparison of glial cells across model systems (**Fig. 4A**), characterization of *in vitro* cell cultures (**Fig. 4B**), single cells (**Fig. 4B-C**), or whole organisms (**Fig. 4D**), genetic studies (**Fig. 4B-C**), and the impact of environmental stress on immune signaling and coral reef ecosystems (**Fig. 4D-E**). Manual and AutoMorFi measurements confirmed the hypothesis of reduced dendritic arborization in Ube3a 2x Tg mouse neurons[19–21] which model Ube3a overdosage and hyperactivity in ASD[22–26]. AutoMorFi further unveiled additional morphological changes in the Ube3a 2x Tg neurons (**Fig. 4B**). Cilia are membrane-covered cell protrusions found in ciliated cells involved in facilitating movement or transport of substances. Impaired ciliated cells can lead to asthma, infertility, or hydrocephalus. Formation of cilia requires precise molecular regulation at the centriole to switch from cell division to cilia formation. By combining AutoMorFi results and fluorescence intensity measurements from markers that define and describe multi-ciliated cells (MCCs), we produced fast readouts to understand how modulating molecules such as the centriolar protein Cp110 affects ciliogenesis[27] (**Fig. 4C**). NF-κB proteins are important for many cellular processes including immunity, inflammation, development, cellular growth, and apoptosis. They are differentially regulated in many diseases such as cancer, arthritis, chronic inflammation, asthma, neurodegenerative disease, and heart disease. Starvation of sea anemones reduces NF-κB and leaves them vulnerable to infection[28]. By reanalyzing the images used in the study using AutoMorFi and taking intensity measurements of NF-κB, we validated the earlier findings and discovered in addition that starvation does not alter the gross morphology or NF-κB distribution in these animals (**Fig. 4D**). Coral reefs are critically threatened by climate change. Recent advancements in sequencing for non-model systems have revealed previously unrecognized ‘cryptic coral lineages’ (*i.e.,* genetically distinct but morphologically similar taxa) that have important implications for predicting reef ecosystem futures and effectively restoring reefs[29]. Rapid and cost-effective methods to identify these cryptic lineages, preferably alternative methods to DNA sequencing, are needed to effectively characterize coral diversity present on reef ecosystems and ultimately improve lineage

assignment. AutoMorFi identified diagnostic skeletal phenotypes and replicated the same pattern of cryptic lineage differentiation in much less time compared to previous analysis requiring ~25 minutes per image to measure all relevant traits (**Fig. 4E**).

In summary, we have demonstrated the easy application and versatility of AutoMorFi for rapid and reproducible acquisition of morphometric data across biological scales and research objectives. We have considered various pitfalls identified through thorough executions of AutoMorFi by multiple research teams and provided a troubleshooting guide (**Supplementary Information 3**) to promote broad usage and customization of the tool for novel applications. For example, AutoMorFi could be adapted to quantify and classify condensates of cellular proteins undergoing liquid-liquid phase separation to introduce more quantitative descriptors of proteostasis in disease and aging to the field[30]. Using AutoMorFi, experimental power is easily increased due to unlimited and unbiased sampling. When applied to multi-channel images and combined with additional approaches such as genetics and genomics as well as other classification algorithms (e.g., random forest), morphometrics will serve as potent indicators and predictors of disease states and environmental changes.

ACKNOWLEDGEMENTS

The authors thank AutoGliji beta testers C. Reddy, E. Choi, K. Sampat, E. Kraft, V. Chiplunkar, M. Iordanov, S. Guerra, K. He, H. LeBlanc, J. Koo, M. Zreik, P. Ruiz, S. Brayton, S. Jo, T. Keefauver, A. Hoo, E. Batchelor, E. Maloney, C.H. Cheng, and A. Liu, and I. Amin for assistance with microscopy. *In memoriam* M. Spelleken and Scarlet. T.L.T. was supported by a NARSAD Young Investigator Grant from the Brain & Behavior Research Foundation, Spivack Neuroscience Pilot Award, and Patricia McLellan Leavitt Research Fund Award.

AUTHOR CONTRIBUTIONS

Z.M., D.B., C.Y., and O.B. established the macro. C.Y. wrote the program to match coordinates. O.B., J.Z., C.Y., N.I., J.Y., A.V.M., C.J.III, J.C., C-Y.C., T-C.H., B.P., M.H., G.L., E.K., E.Z., H.A., S.D., P.W., Y.T., H.M., E.O., K.H., T.G., and D.P. generated data, provided validated images, and/or performed analyses. O.B. and T.L.T. wrote the manuscript. T.L.T. conceived and supervised the study.

164 **COMPETING INTERESTS**

165 The authors declare no competing interests.

166 **MATERIAL AND METHODS**

167 **Sample preparation.**

168 **Mouse.** Female C57Bl/6J (wild-type) mice were purchased from Charles River Laboratories and
169 raised in a specific-pathogen-free facility under 10h/14h dark/light cycle until 52 weeks old. Mice
170 were given food and water *ad libitum*. Animal experiments are approved by the Institutional Animal
171 Care and Use Committee (IPROTO202200000054). Mice were deeply anesthetized by
172 intraperitoneal administration of 100 mg ketamine and 5 mg xylazine per kg body weight and
173 transcardially perfused with phosphate-buffered saline (PBS). Brains, hearts, kidneys, livers,
174 lungs, and spleens were post-fixed overnight at 4°C in 4% paraformaldehyde (PFA) in PBS, rinsed
175 in PBS, and cryoprotected in 30% sucrose/PBS at 4°C until fully submerged. Samples were
176 embedded in Tissue-Tek O.C.T. compound (Sakura Finetek, USA) for frozen sectioning on a
177 cryostat (Cryostar NX50; Epredia Cryostat, USA).

178 **Human.** Human postmortem brain tissues from 2 MS and 2 control patients were obtained
179 according to an institutional review board-approved protocol (Yale HIC 1211011031) (**Table 2**).
180 Brain hemispheres were fixed with formalin for a minimum of 2 weeks. Brain slabs with lesions
181 were embedded with paraffin. A chronic active MS lesion was characterized using brightfield
182 staining. Images of human postmortem tissue from the dorsolateral frontal cortex were obtained
183 from the Boston University Alzheimer's Disease Research Center (BU ADRC): 5 cases from 3
184 females and 2 males aged 75–105 with either a non-AD or low NIA-Reagan score, and with no
185 other comorbid pathology were taken for the control group.

186 **Human iPSC-derived microglia.** A trisomic line (WC-24-02-DS-M) and an isogenic euploid
187 control cell line (WC-24-02-DS-B) between passages 18 and 27 were generated from a female
188 25-year-old with Down syndrome and used in this study. The cell lines were produced, validated,
189 and kindly provided by Dr. Anita Bhattacharyya from the University of Wisconsin-Madison. IPSCs
190 were routinely passaged and cultured on Matrigel® (cat. 354277 Corning®, Corning, NY, USA)
191 using mTeSR™ plus (cat. 85850, StemCell Technologies, Vancouver, BC, Canada). To generate
192 iPSC derived microglia, iPSCs were differentiated into CD-43 expressing hematopoietic
193 progenitor cells (HPCs) using the STEMdiff™ Hematopoietic Kit (cat. 05310, STEMCELL
194 Technologies) for 12 days. The expression of CD43, CD45, and CD34 was validated by flow
195 cytometry. Cells expressing >90% $CD43^+$ and >20% of $CD34^+/CD45^+$ on day 12 were confirmed
196 to be HPCs, cryoprotected, and used for the subsequent differentiation into microglia. The

197 microglial differentiation was performed on thawed HPCs (200,000 cells per well of a 6-well plate)
198 using the STEMdiff™ Microglia Culture System (cat. 100-0019 and 100-0020, STEMCELL
199 Technologies) for 24 days according to manufacturer's directions. On day 24, expression of >80%
200 $CD45^+$ and $CD11b^+$ microglial markers was confirmed by flow cytometry to ensure proper
201 differentiation. Cells were plated on poly-d-lysine coated glass coverslips (cat. A3890401,
202 ThermoFisher, Waltham, MA, USA) at 100,000 cells/well and matured until day 30. Cells were
203 fixed with 4% PFA for 30 min, washed twice with PBS, and stored at 4°C until use.
204 **Primary neuronal culture.** Primary neuronal cultures were prepared from postnatal day 0 (P0)
205 mouse pups. At P0, brain tissues from WT and Ube3a 2x Tg male pups were dissected and
206 digested, and then plated onto circular coverslips for neuron culture.
207 ***Drosophila*.** Fly strains *alrm-GAL4* (#67032) and *UAS-IVS-GFP* (#32201) were obtained from the
208 Bloomington *Drosophila* Stock Center, crossed at 25˚C, and raised at 29˚C on standard cornmeal
209 and molasses food. Flies aged to 2 days were dissected for immunohistochemistry. Only male
210 flies were included in the experiment.
211 **Sea anemone.** *Nematostella vectensis* (*Nv*) were obtained from Maryland by Mark Martindale
212 and Matt Gibson. The anemones were kept at ⅓ strength artificial seawater (ASW, ~12 parts per
213 1000) in a dark incubator at 19°C with weekly water changes. Clonal pairs of *Nv* were generated
214 by bisection and regeneration and then fed or starved for 30 days. Adult animals were bisected
215 perpendicularly to the oral-aboral axis. Halves were placed in wells of a 24-well plate. Anemones
216 regenerated for 30 days with feeding paused until tentacles formed from the aboral end. Adult *Nv*
217 were fed freshly hatched brine shrimp (*Artemia*; brineshrimpdirect.com) and young polyps were
218 fed ground *Artemia* in ⅓ ASW three times a week. Animals that were regenerated from aboral
219 and oral ends were included. 40-day-old polyps that were fed or starved for 30 days were used.
220 ***Xenopus*.** MCCs of mucociliary epithelia of *Xenopus* embryos were used to explore cilia
221 formation. MCCs form >100 basal bodies and motile cilia that are important for generating
222 directional fluid flow for mucus clearance from the airways or the tadpole skin. Embryos were
223 injected with morpholino oligonucleotide (MO) to induce knockdown of *cp110* to study the role of
224 cp110 in MCC ciliogenesis. Some of the *cp110*MO-injected embryos were co-injected with *cp110*
225 DNA to rescue cilia formation. *Centrin4-cfp* was injected into embryos to identify targeted MCCs.
226 **Corals.** *Siderastrea siderea* (massive starlet coral) is one of the primary reef-building corals in
227 Bocas del Toro, Panamá[31,32]. Previous work identified three cryptic lineages of *S. siderea* that
228 occupy sites spanning the inshore reefs of Bocas del Toro[33].
229
230 **Immunohistochemistry.**

231 **Mouse.** Sagittal sections of brains, hearts, and kidneys and sections of livers, lungs and spleens
232 were captured at 16-μm thickness on Superfrost™ slides and stored at -20°C until use. Tissue
233 sections were rehydrated using PBS and permeabilized in blocking solution containing 0.5%
234 Triton-X-100 (Sigma Aldrich, USA) and 5% bovine serum albumin (BSA) (Sigma Aldrich, USA) in
235 PBS for 1 h at room temperature (RT). Tissues were incubated overnight at 4°C with rabbit anti-
236 IBA1 antibody (1:500; Wako 019-19741) diluted in PBS containing 0.1% Triton-X-100 (Sigma
237 Aldrich, USA) and 5% BSA (Sigma Aldrich, USA). After 5 10-min rinses in PBST, tissues were
238 incubated with Alexa Fluor 647-conjugated donkey anti-rabbit secondary antibody (1:1000;
239 Thermofisher Scientific A-31573) at RT for 2 h. After 5 10-min rinses in PBST, tissues were
240 coverslipped with Prolong Gold Antifade Mountant containing 4′,6-diamidino-2-phenylindole
241 (DAPI) (Cell Signaling, 8961).
242 **Human.** PLP was used to identify the areas of MS lesion and CD68 was used to identify the active
243 rim of microglial cells (**Table 2**). For fluorescent staining, the formalin-fixed paraffin embedded
244 (FFPE) block was sectioned at 7-μm thickness onto a slide, deparaffinized in xylene and
245 rehydrated via an ethanol series. The section was subjected to antigen retrieval using citrate
246 buffer at pH 6.0 followed by permeabilization using 0.5% Triton X-100 in Tris-buffered saline
247 (TBS). After washing, the section was quenched in 0.3% H_2O_2 in TBS and washed again. Tissue
248 was blocked for 1 h using 10% normal goat serum (NGS) and 10% Fc receptor inhibitor
249 (Invitrogen, 14-9161-73) in TBS. Primary antibody for IBA-1 (Synaptic Systems, #234004) was
250 applied with 10% NGS and incubated at 4°C overnight. After several washes in TBST, Alexa-
251 Fluor 488-conjugated secondary antibody (Invitrogen, #A1073) was applied at RT for 3 h. After
252 several washes, Sudan Black (MP Biomedicals, 152088) was applied to reduce autofluorescence,
253 followed by washes and Hoechst Counterstain (Life Technologies, H357). Slices were
254 coverslipped with 50% glycerol in TBS. Paraffin-embedded brain tissues from the BU ADRC were
255 cut at 20-μm thickness. DAB (3, 3'-diaminobenzidine) immunohistochemical staining for IBA-1
256 (1:500, Wako, 019-19741) and nuclear counterstaining with hematoxylin was performed.
257 **Human iPSC-derived microglia.** Glass coverslips were treated with blocking solution containing
258 5% normal donkey serum in PBST (0.1% Triton X-100) at RT for 1 h. Cells on coverslips were
259 incubated overnight at 4°C in rabbit anti-IBA1 (1:500; Wako, 019-19741) diluted in blocking
260 solution. Coverslips were washed 3X for 10 min in PBST and incubated at RT for 1 h with Alexa-
261 Fluor 546-conjugated donkey anti-rabbit antibody (1:1000; Invitrogen, A10040) in blocking
262 solution. Coverslips were washed 3X 10 min in PBST. ProLong Gold Antifade Mountant with DAPI
263 (Invitrogen, P36931) was applied to adhere coverslips to slides. Slides were stored at 4°C and
264 light-protected until imaging.

265 **Primary neuronal culture.** Neurons plated on coverslips were fixed at day *in vitro* 8 (DIV8) in 4%
266 PFA for 8 min and washed twice in 1X PBS. Cells were permeabilized for 10 min in 0.3% Triton
267 X-100 (Sigma) in 1X PBS, followed by 2 washes in 1X PBS. Cells were blocked for 1 h in 10%
268 NGS in 1X PBS. To label dendritic structures, cells were incubated overnight at 4°C in 1X PBS
269 containing MAP2 monoclonal antibody (1:300; ThermoFisher, #13-1500). The next day, cells
270 were washed 3X with cold 1X PBS, followed by incubation in 1X PBS containing Alexa Fluor 488
271 or 555-conjugated mouse IgG secondary antibody (1:500; Invitrogen, #A-21422. Cells were
272 counterstained with Hoechst (1:10,000 in 1X PBS; ThermoFisher, H3570) for 30 sec followed by
273 2 washes in 1X PBS. Coverslips were mounted onto slides with Prolong Gold (ThermoFisher,
274 P36930) and left to dry in the dark overnight before imaging.
275 ***Drosophila.*** Male flies were fixed in 4% PFA diluted in 1X PBS and 0.5% Triton X-100 (PBT) at
276 RT for 3 h. Flies were washed 4X in PBT for 15 min each with rotation and dissected in PBS.
277 Whole brains were blocked at RT for 1 h in PBT containing 0.5% BSA and 5% NGS (PBANG)
278 and then incubated in PBANG containing rabbit anti-GFP (1:100; Torry Pines Biolabs, TP401) at
279 4˚C for 2 nights. Brains were washed 4X in PBT at RT and incubated in PBANG containing goat
280 anti-rabbit Cy3 (1:200; Jackson ImmunoResearch, 111-165-003) for 2 nights at 4˚C. Brains were
281 washed 3X in PBT. Samples were placed in VectaShield with DAPI (Vector Labs) overnight at
282 4°C and subsequently mounted on slides.
283 **Sea anemone.** Whole-mount immunofluorescence staining of NF-κB was performed using a
284 custom antibody and Texas Red-labeled secondary antibody to visualize NF-κB levels in *Nv*. For
285 immunofluorescence, *Nv* polyps were fixed in 4% formaldehyde in ⅓ ASW overnight at 4°C and
286 then washed 3X with 0.1% Triton X-100 in PBS (PTx). Polyps were then microwaved in warm
287 urea (5% w/v) at the lowest setting for 5 min, cooled at RT for 20 min, then washed 3X with PTx.
288 Polyps were blocked overnight in PTx containing 5% NGS and 1% BSA at 4°C on a nutator. Anti-
289 Nv-NF-κB antibody diluted 1:100 in blocking buffer was used overnight at 4°C. Polyps were
290 washed 4X with PTx and incubated in Texas-red-conjugated anti-rabbit secondary antibody
291 (1:160; Invitrogen, #T-2767). DAPI was added to a final concentration of 5 mg/ml to visualize
292 nuclei.
293 ***Xenopus.*** Whole embryos were fixed at embryonic stages 30-32 overnight at 4°C, washed 3X 15
294 min with PBS, 2X 30 min in PBST (0.1% Triton X-100 in PBS), and blocked at RT in PBST-CAS
295 (CAS blocking; ThermoFisher #00-8120) for 1 h. To visualize cilia, embryos were incubated
296 overnight at 4°C in mouse monoclonal anti-acetylated-α-tubulin antibody (1:700; Sigma, #T6793)
297 and Alexa Fluor 555-labeled goat anti-mouse antibody (1:250; Molecular Probes, #A21422) in
298 CAS Blocking.

299

300 **Image acquisition and processing.**

301 **Mouse.** Z stacks of whole organ sections were acquired on a ZEISS AxioScan 7 slide scanner
302 using a 20X 1 NA objective lens at 1X zoom and 1.1 binning. Images were sampled with a voxel
303 size of 0.325-µm X 0.325-µm X 1-µm for the DAPI (excitation wavelength 353-nm; emission
304 wavelength 465-nm) and Alexa Fluor 647 (excitation wavelength 650-nm; emission wavelength
305 665-nm) channels. Image tiles were stitched, processed for maximum intensity projections
306 (MIPs), cropped to obtain >200 cells per image, and exported as TIFF images using the ZEISS
307 ZEN pro software (ZEN 3.2 blue edition). At least 4 images were analyzed per organ/mouse.

308 **Human.** Tissue sections from MS patients were scanned on a Leica Microsystems DM6B
309 microscope a 40X objective lens at 0.329-µm per pixel. Each tile was focused using the "Auto-
310 focus" function and subsequently captured in multiple z-stack images of 6-µm thickness in total.
311 Z-interval was set depending on tissue quality. Tiled images were merged with the "Mosaic
312 merge" function to include a 20% overlay area. The "Projection" function was used to obtain MIPs
313 that contained the best signal intensity for each pixel. Images were cleaned up using "Instant
314 Computational Cleaning" under the "Thunder" function before they were exported in TIFF for
315 image processing in ImageJ. Images were aligned with the function "Registration".
316 Autofluorescence was subtracted using the "Image Calculator". A signal threshold was set to
317 preserve regions above a defined intensity. Particles smaller than the size of a cell were discarded
318 using "Particle Remover". "Watershed" or "Erode" were employed to separate connected cells
319 that were extracted with "Analyze Particles" and "Image Calculator". The separated cells were
320 subsequently added back to the original image with the "Image Calculator". Images containing
321 MS lesions were characterized by PLP, CD68, and IBA1 expression and precisely cropped for
322 morphometric analysis. Tissue sections from BU ADRC were imaged using an Aperio GT450
323 slide scanner at a 40X magnification. Images were processed using the "extract region tool" in
324 the Aperio ImageScope Pathology Slide Viewing Software to generate 3 cropped images
325 measuring <1000-µm X 1000-µm each from the white and gray matter. To minimize the noise
326 contributed by the nuclear counterstain, thresholding and subtraction of the nuclear signals using
327 the "Threshold" and "Image Calculator" functions were performed in ImageJ/Fiji to generate a
328 new 8-bit TIFF image for subsequent analysis.

329 **Human iPSC-derived microglia.** Images were acquired on an Olympus Fluoview FV300 using
330 a 40X oil immersion objective lens and the FV31S-SW Viewer software. Images were captured in
331 DAPI (excitation wavelength 353-nm; emission wavelength 465-nm) and Alexa-Fluor 546
332 (excitation wavelength 556-nm; emission wavelength 573-nm) channels.

333 **Primary neuronal culture.** Neuronal images were captured using a Carl Zeiss Axiovert inverted
334 fluorescence microscope with a 40X 1.3 NA oil immersion objective lens and the AxioVision
335 Release 4.5 software.
336 ***Drosophila*.** Images of the central brain were captured on a Nikon C2+Si confocal microscope
337 using a 40X 1.25 NA water immersion objective lens and NIS-Elements software. Fifty planes 1-
338 µm apart were captured for the Z stacks of each brain with a resolution of 1024 X 1024 pixels
339 starting from the surface of the central brain at the first point where the antennal lobe becomes
340 visible. MIPs were generated in ImageJ at serial steps of 10 (e.g., 1-10, 11-20, …, and 41-50) to
341 distinguish individual glial cells in each brain.
342 **Sea anemone.** Images were acquired on a Nikon C2 Si confocal microscope and processed
343 using ImageJ.
344 ***Xenopus.*** Images were acquired using a ZEISS LSM700 confocal microscope. ImageJ was used
345 for Z-stack analysis and processing.
346 **Corals.** Photos of representative coral colonies of each of the three cryptic lineages were taken
347 from three sites across Bocas del Toro (Hospital Point, Cristobal Island, and STRI Point) using
348 an Olympus Tough TG-6 camera on the underwater macro setting. For each individual coral (N =
349 52), macro photos focused on individual corallites were taken in triplicate, with each of the three
350 photos taken on a different location on the coral surface. A size standard was included in each
351 photograph.
352
353 **AutoMorFi morphometric analysis of single cells.** Images were blinded before the individuals
354 who did not generate the primary data ran the AutoMorFi macro except for iPSC-derived
355 microglial cells and *Drosophila* astrocyte-like glia which were known to the persons who
356 performed image analysis. A different set of individuals performed quality control to validate the
357 AutoMorFi output. They compared the outlines of the detected “soma” and “whole cell” with cells
358 in the original images to assess for false positive or false negative detections and inaccurate
359 object segmentation in consultation with authors of the original experiments. Incorrectly detected
360 cells or objects were removed from the .csv output files. Output images with missing cells were
361 reanalyzed using improved diameter measurements. Procedures for running the AutoMorFi
362 macro in ImageJ/Fiji are detailed in **Supplementary Information 1–3**. Each single-cell
363 measurement of “soma”, “whole cell”, and “skeletonized” structure (generated by ImageJ/Fiji from
364 the whole-cell outline) derived from AutoMorFi were matched by the coordinates of the objects
365 using the Python packages numpy, pandas, and sklearn.neighbors, and collated in a single .csv
366 data file. AutoMorFi generated 33 morphometric measurements that were in part used in

367 arithmetic functions that produced additional parameters resulting in a total of 47 quantitative
368 characteristics per cell (**Table 1**).
369
370 **AutoMorFi morphometric analysis of single objects.** Image blinding and data validation were
371 carried out as described for AutoMorFi analysis of single cells. To customize AutoMorFi for
372 measuring non-cellular objects, the use of the pipeline was modified as follows.
373 **Sea anemone.** The diameters of several whole polyps were measured from the DNA channel to
374 obtain a range of representative values. While executing AutoMorFi, the Analyze Particle plugin
375 was set to “Overlay” instead of “Mask” to save the polyp outline as an overlay that was now
376 considered the "whole cell". The overlay was renamed and manually saved as a TIFF image in
377 the output folder before continuing with the AutoMorFi macro. A region of interest (ROI) was
378 marked in the background of the image and added to the ROI manager to generate a second
379 pseudo-object to allow the acquisition of all standard parameters of the whole single polyp (see
380 Error 6 in **Supplementary Information 3**). The macro was continued until the end.
381 Measurements from the marked ROI and "soma" were excluded from the data analysis. “Whole
382 cell” and “skeletonized” objects based on whole-polyp outlines contributing to 21 measured
383 parameters were matched by their coordinates and collated in a single .csv data file. To acquire
384 the total fluorescence intensity measurement of DNA and NF-κB signals, the overlay outline or
385 "whole cell outline" that was saved earlier was added to the ROI manager in ImageJ/Fiji for each
386 individual channel per organism. The measured total fluorescence intensity values were
387 normalized to the polyp area within the whole cell outline. The NF-κB area fraction represents the
388 percentage of non-zero pixels within the polyp outline. An additional 12 calculated parameters
389 (**Table 1**: 34, 35, 38, 39, 40, 41, 42, 46, 47; total DNA fluorescence intensity, total NF-κB
390 fluorescence intensity, and NF-κB area fraction) resulted in a total of 33 quantitative
391 characteristics per polyp.
392 ***Xenopus.*** Focusing only on the acetylated-α-tubulin channel of the imaged MCCs, diameters of
393 several representative objects indicated by acetylated-α-tubulin staining were measured across
394 images to obtain a range of values for running the AutoMorFi macro. Measurements of "soma"
395 were excluded. “Whole cell” and “skeletonized” outlines were matched by their coordinates. Total
396 acetylated-α-tubulin fluorescence intensity was measured for each MCC. By including the
397 calculated parameters (**Table 1**: 34, 35, 38, 39, 40, 41, 42, 46, 47, and total acetylated-α-tubulin
398 fluorescence intensity), a total of 31 quantitative characteristics was obtained per MCC.
399 **Corals.** Representative diameters of several corallites were acquired across coral lineages.
400 Measurements of incomplete corallites, corallites covered by sand, and “somas” were excluded.

401 “Whole cell” and “skeletonized” parameters contributed to 21 morphometric measurements.
402 Additional calculated parameters (**Table 1**: 34, 35, 38, 39, 40, 41, 42, 46, and 47) resulted in a
403 total of 30 quantitative characteristics per corallite.
404
405 **Data visualization.** Unpaired t-tests, pairwise comparisons of morphometric parameters, and
406 principal component analysis (PCA) were performed between or across groups to determine the
407 need for dimensionality reduction[5,34] using tidyverse, ggplot2, and pheatmap R packages.
408 Redundant morphometric features with high correlation coefficients between 0.5 and 1 were
409 removed to mitigate bias in subsequent cluster analysis. Unsupervised K-means clustering
410 analysis was performed on the reduced datasets using the R factoextra package. For data
411 visualization, UMAPs were generated using tidyverse, dplyr, ggplot2, and umap R packages, and
412 heatmaps were generated using dplyr, ggplot2, and pheatmap R packages in R.4.3.2.
413
414 **Statistical analysis.** Paired and unpaired t-tests were performed using GraphPad Prism10. Data
415 are presented as mean ± s.e.m. and considered statistically significant at $p < 0.05$.

REFERENCES

1. Cajal, S. R. y. *Degeneration & Regeneration of the Nervous System*. (Oxford University Press, Humphrey Milford, 1928).
2. Lawson, L. J., Perry, V. H., Dri, P. & Gordon, S. Heterogeneity in the distribution and morphology of microglia in the normal adult mouse brain. *Neuroscience* **39**, 151–170 (1990).
3. Sierra, A. *et al.* The “Big-Bang” for modern glial biology: Translation and comments on Pío del Río-Hortega 1919 series of papers on microglia: 1919 Río-Hortega Papers on Microglia. *Glia* **64**, 1801–1840 (2016).
4. Falk, T. *et al.* U-Net: deep learning for cell counting, detection, and morphometry. *Nat. Methods* **16**, 67–70 (2019).
5. Colombo, G. *et al.* A tool for mapping microglial morphology, morphOMICs, reveals brain-region and sex-dependent phenotypes. *Nat. Neurosci.* **25**, 1379–1393 (2022).
6. Karbstein, K. *et al.* Species delimitation 4.0: integrative taxonomy meets artificial intelligence. *Trends Ecol. Evol.* (2024) doi:10.1016/j.tree.2023.11.002.
7. Reddaway, J., Richardson, P. E., Bevan, R. J., Stoneman, J. & Palombo, M. Microglial morphometric analysis: so many options, so little consistency. *Front. Neuroinformatics* **17**, (2023).
8. Schindelin, J. *et al.* Fiji: an open-source platform for biological-image analysis. *Nat. Methods* **9**, 676–682 (2012).
9. Schneider, C. A., Rasband, W. S. & Eliceiri, K. W. NIH Image to ImageJ: 25 years of image analysis. *Nat. Methods* **9**, 671–675 (2012).
10. Boulan, B. *et al.* AutoNeuriteJ: An ImageJ plugin for measurement and classification of neuritic extensions. *PLoS ONE* **15**, e0234529 (2020).
11. Longair, M. H., Baker, D. A. & Armstrong, J. D. Simple Neurite Tracer: open source software for reconstruction, visualization and analysis of neuronal processes. *Bioinformatics* **27**, 2453–2454 (2011).

442 12. Donadon, M. *et al.* Macrophage morphology correlates with single-cell diversity and prognosis
443 in colorectal liver metastasis. *J. Exp. Med.* **217**, e20191847 (2020).
444 13. Donovan, K. M. *et al.* Allograft Inflammatory Factor 1 as an Immunohistochemical Marker for
445 Macrophages in Multiple Tissues and Laboratory Animal Species. *Comp. Med.* **68**, 341–348
446 (2018).
447 14. Hagemeyer, N. *et al.* Transcriptome-based profiling of yolk sac-derived macrophages reveals
448 a role for Irf8 in macrophage maturation. *EMBO J.* **35**, 1730–1744 (2016).
449 15. Voet, S., Prinz, M. & van Loo, G. Microglia in Central Nervous System Inflammation and
450 Multiple Sclerosis Pathology. *Trends Mol. Med.* **25**, 112–123 (2019).
451 16. Yong, V. W. Microglia in multiple sclerosis: Protectors turn destroyers. *Neuron* **110**, 3534–
452 3548 (2022).
453 17. Zia, S. *et al.* Microglia Diversity in Health and Multiple Sclerosis. *Front. Immunol.* **11**, 588021
454 (2020).
455 18. Prineas, J. W. & Lee, S. Microglia subtypes in acute, subacute, and chronic multiple sclerosis.
456 *J. Neuropathol. Exp. Neurol.* **82**, 674–694 (2023).
457 19. Khatri, N. *et al.* The Autism Protein Ube3A/E6AP Remodels Neuronal Dendritic Arborization
458 via Caspase-Dependent Microtubule Destabilization. *J. Neurosci. Off. J. Soc. Neurosci.* **38**,
459 363–378 (2018).
460 20. Smith, S. E. P. *et al.* Increased gene dosage of Ube3a results in autism traits and decreased
461 glutamate synaptic transmission in mice. *Sci. Transl. Med.* **3**, 103ra97 (2011).
462 21. Krishnan, V. *et al.* Autism gene Ube3a and seizures impair sociability by repressing VTA
463 Cbln1. *Nature* **543**, 507–512 (2017).
464 22. Hogart, A., Wu, D., LaSalle, J. M. & Schanen, N. C. The comorbidity of autism with the
465 genomic disorders of chromosome 15q11.2-q13. *Neurobiol. Dis.* **38**, 181–191 (2010).

466 23. Khatri, N. & Man, H.-Y. The Autism and Angelman Syndrome Protein Ube3A/E6AP: The
467 Gene, E3 Ligase Ubiquitination Targets and Neurobiological Functions. *Front. Mol. Neurosci.*
468 **12**, 109 (2019).
469 24. Yi, J. J. *et al.* An Autism-Linked Mutation Disables Phosphorylation Control of UBE3A. *Cell*
470 **162**, 795–807 (2015).
471 25. Iossifov, I. *et al.* The contribution of de novo coding mutations to autism spectrum disorder.
472 *Nature* **515**, 216–221 (2014).
473 26. Weston, K. P. *et al.* Identification of disease-linked hyperactivating mutations in UBE3A
474 through large-scale functional variant analysis. *Nat. Commun.* **12**, 6809 (2021).
475 27. Walentek, P. *et al.* Ciliary transcription factors and miRNAs precisely regulate Cp110 levels
476 required for ciliary adhesions and ciliogenesis. *eLife* **5**, e17557 (2016).
477 28. Carrión, P. J. A. *et al.* Starvation decreases immunity and immune regulatory factor NF-κB in
478 the starlet sea anemone Nematostella vectensis. *Commun. Biol.* **6**, 698 (2023).
479 29. Grupstra, C. G. B. *et al.* Integrating cryptic diversity into coral evolution, symbiosis and
480 conservation. *Nat. Ecol. Evol.* **8**, 622–636 (2024).
481 30. Scott-Hewitt, N. *et al.* Microglial-derived C1q integrates into neuronal ribonucleoprotein
482 complexes and impacts protein homeostasis in the aging brain. *Cell* **187**, 1–20 (2024).
483 31. Seemann, J. *et al.* Assessing the ecological effects of human impacts on coral reefs in Bocas
484 del Toro, Panama. *Environ. Monit. Assess.* **186**, 1747–1763 (2014).
485 32. Guzmán, H. M. & Guevara, C. A. [Coral reefs of Bocas del Toro, Panamá: IV. Distribution,
486 structure and conservation state of continental reefs of Peninsula Valiente]. *Rev. Biol. Trop.*
487 **49**, 53–66 (2001).
488 33. Aichelman, H. E. Exploring coral symbiosis under climate change stress across spatial and
489 temporal scales. (2023).
490 34. van Weering, H. R. J., Nijboer, T. W., Brummer, M. L., Boddeke, E. W. G. M. & Eggen, B. J.
491 L. Microglia morphotyping in the adult mouse CNS using hierarchical clustering on principal

492 components reveals regional heterogeneity but no sexual dimorphism. *Glia* **71**, 2356–2371
493 (2023).

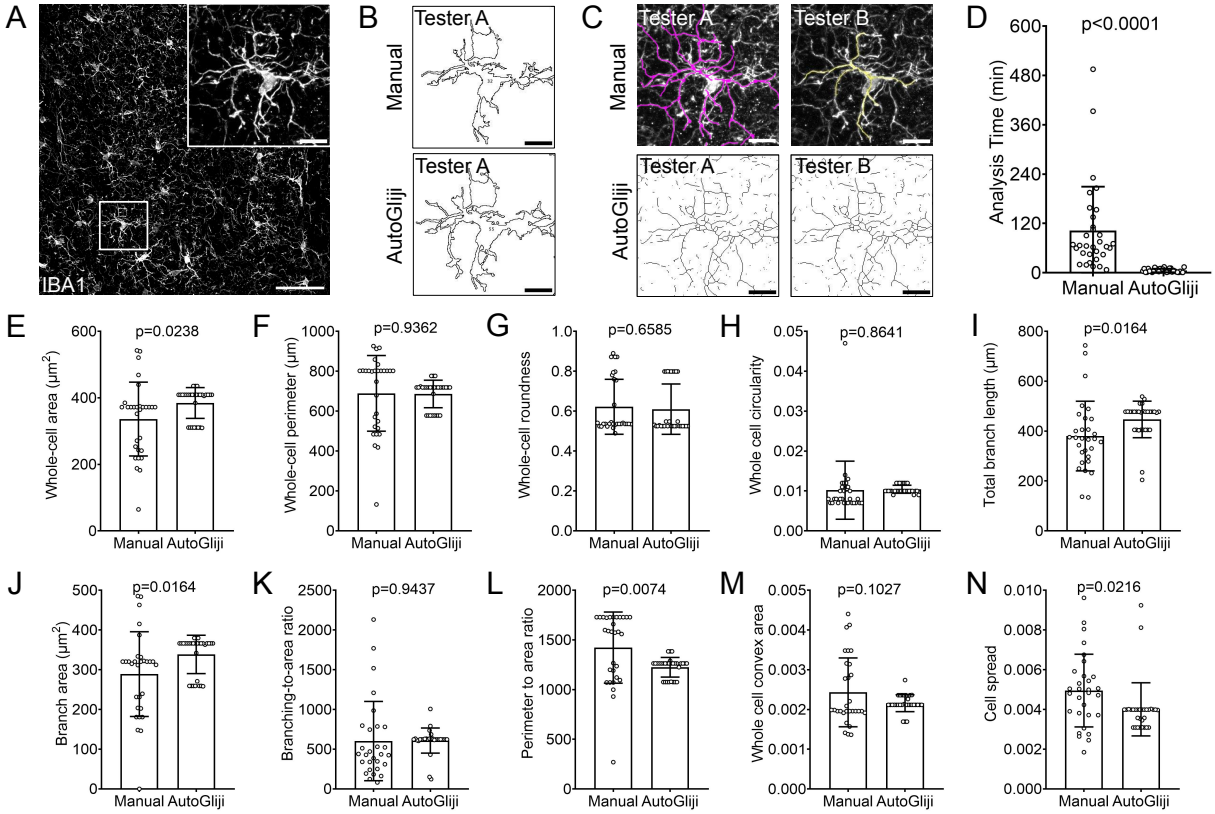

Figure 1: Acquisition and validation of whole-image cell morphometric data using the AutoMorFi prototype, AutoGliji. (A) Widefield fluorescence image of IBA-1-immunolabeled mouse cortical microglia (white) used for manual and automated morphometric analysis of 3 selected cells by 30 testers. Inset shows cell #3 corresponding to data in **B-N**. **(B)** Representative manual and automated cell thresholding and detection by 1 tester. **(C)** Representative manual trace using Simple Neurite Tracer and automated cell traces using AutoGliji by 2 testers. **(D)** Total time taken per tester for manual and automated data acquisition for cells #1–3. **(E-N)** Examples of manual and automated morphometric measurements of cell #3 for **(E)** whole-cell area, **(F)** whole-cell perimeter, **(G)** whole-cell roundness, **(H)** whole-cell circularity, **(I)** total branch length, **(J)** branch area, **(K)** branching to area ratio, **(L)** perimeter to area ratio, **(M)** whole cell convex area, and **(N)** cell spread. **(D-N)** Data are represented as mean ± s.e.m. Paired t-test. *N* = 30. Scale bars, 100 μm (overview in **A**); 10 μm (inset in **A**, **B**, and **C**).

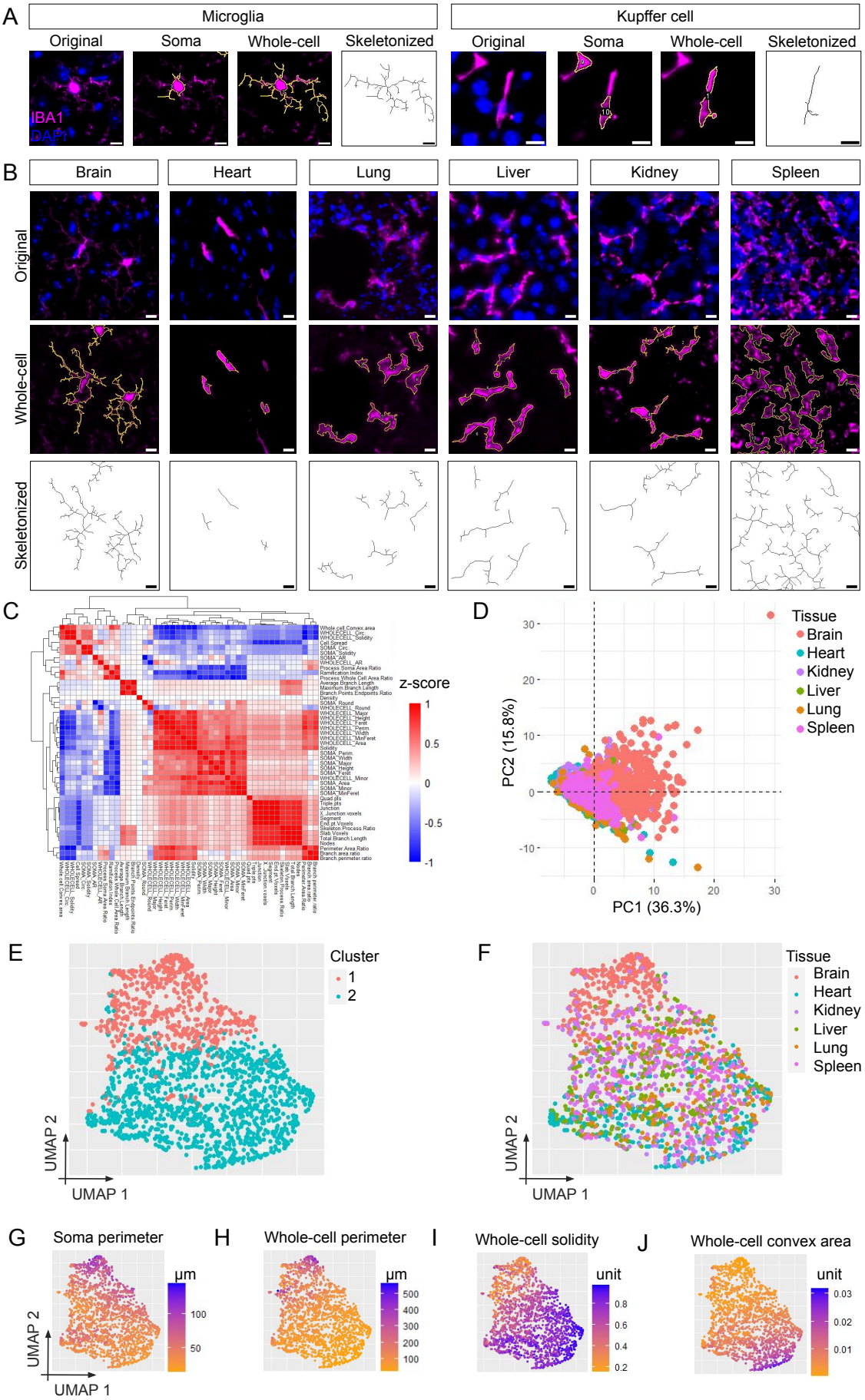
A
Microglia
Kupffer cell
Original
Soma
Whole-cell
Skeletonized
IBA1
DAPI
B
Brain
Heart
Lung
Liver
Kidney
Spleen
Original
Whole-cell
Skeletonized
C
z-score
1
0.5
0
-0.5
-1
D
Tissue
Brain
Heart
Kidney
Liver
Lung
Spleen
PC2 (15.8%)
PC1 (36.3%)
E
Cluster
1
2
UMAP 2
UMAP 1
F
Tissue
Brain
Heart
Kidney
Liver
Lung
Spleen
UMAP 2
UMAP 1
G
Soma perimeter
μm
100
50
UMAP 2
UMAP 1
H
Whole-cell perimeter
μm
500
400
300
200
100
I
Whole-cell solidity
unit
0.8
0.6
0.4
0.2
J
Whole-cell convex area
unit
0.03
0.02
0.01

Figure 2: Morphometric analysis of tissue-resident macrophages. (A) Representative widefield fluorescence images of IBA-1$^+$ brain-resident microglia and liver Kupffer cells and corresponding elements generated by AutoMorFi including soma outline, whole-cell outline, and skeletonized structure of the whole-cell outline. **(B)** Representative images of homeostatic mouse IBA-1$^+$ tissue-resident macrophages and their corresponding whole-cell outlines and skeletonized traces. **(C)** Correlation matrix of the 47 parameters from AutoMorFi across 1,945 tissue-resident macrophages. **(D)** Principal component analysis (PCA) of 1,945 macrophages based on 47 parameters from AutoMorFi. **(E)** Uniform manifold approximation and projection (UMAP) of 1,945 macrophages in 2 clusters based on 24 morphometric parameters after dimensionality reduction and unsupervised kmeans clustering. **(F)** UMAP of macrophages according to tissue origin. **(G-J)** UMAP of selected parameters, including **(G)** soma perimeter, **(H)** whole-cell perimeter, **(I)** whole-cell solidity, and **(J)** whole-cell convex area. Scale bars, 10 μm.

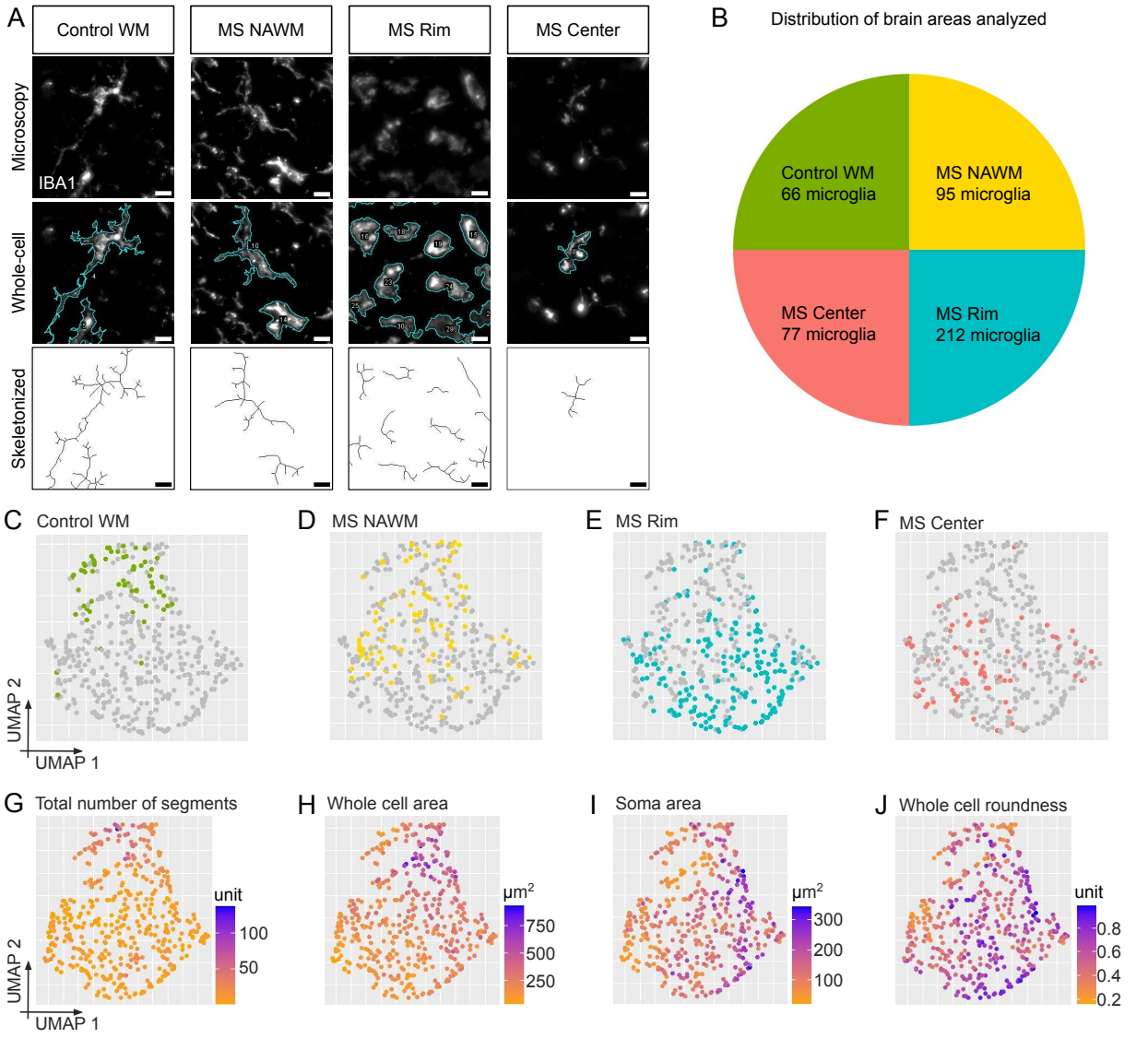

Figure 3: Microglial morphometric analysis in postmortem human MS and control brain. (A) Representative widefield fluorescence images of IBA-1^{+} microglia (white) and their corresponding whole-cell outline and skeletonized trace. **(B)** Microglial cells analyzed from the 4 equally sampled brain areas: control white matter (WM), MS normal-appearing WM (NAWM), MS rim, and MS center. **(C-J)** UMAP of 450 microglia based on 27 morphometric parameters after dimensionality reduction from **(C)** control WM, **(D)** MS NAWM, **(E)** MS rim, and **(F)** MS center and of selected parameters including **(G)** total number of segments, **(H)** whole cell area, **(I)** soma area, and **(J)** whole cell roundness. Scale bars, 10 µm.

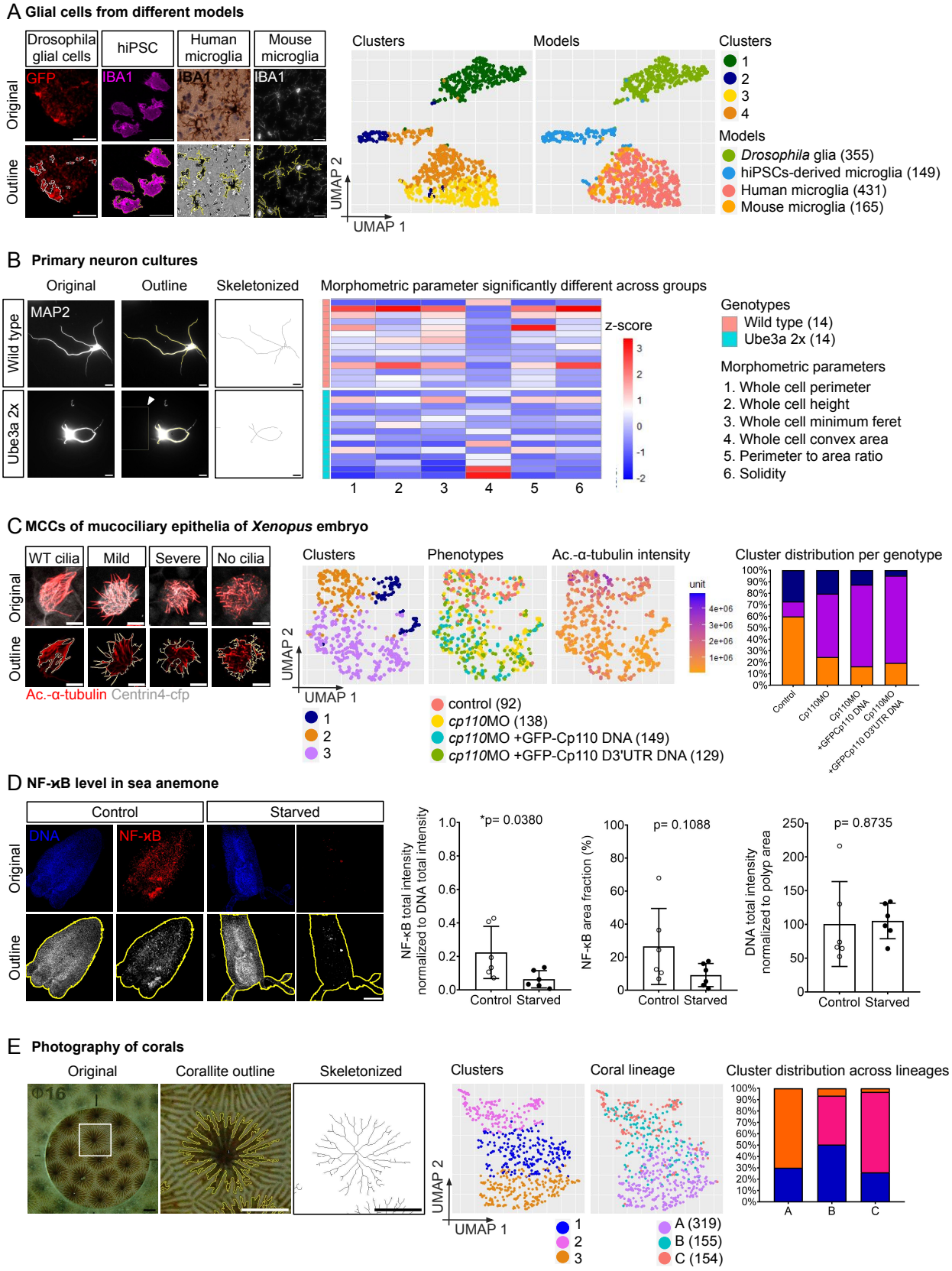
A Glial cells from different models
Drosophila glial cells
hiPSC
Human microglia
Mouse microglia
Original
Outline
GFP
IBA1
Clusters
Models
UMAP 2
UMAP 1
Clusters
1
2
3
4
Models
Drosophila glia (355)
hiPSCs-derived microglia (149)
Human microglia (431)
Mouse microglia (165)
B Primary neuron cultures
Original
Outline
Skeletonized
Morphometric parameter significantly different across groups
Wild type
Ube3a 2x
MAP2
z-score
Genotypes
Wild type (14)
Ube3a 2x (14)
Morphometric parameters
1. Whole cell perimeter
2. Whole cell height
3. Whole cell minimum feret
4. Whole cell convex area
5. Perimeter to area ratio
6. Solidity
C MCCs of mucociliary epithelia of Xenopus embryo
WT cilia
Mild
Severe
No cilia
Ac.-α-tubulin Centrin4-cfp
Clusters
Phenotypes
Ac.-α-tubulin intensity
unit
Cluster distribution per genotype
control (92)
cp110MO (138)
cp110MO +GFP-Cp110 DNA (149)
cp110MO +GFP-Cp110 D3'UTR DNA (129)
D NF-κB level in sea anemone
Control
Starved
DNA
NF-κB
*p= 0.0380
p= 0.1088
p= 0.8735
NF-κB total intensity normalized to DNA total intensity
NF-κB area fraction (%)
DNA total intensity normalized to polyp area
E Photography of corals
Original
Corallite outline
Skeletonized
Clusters
Coral lineage
Cluster distribution across lineages
A (319)
B (155)
C (154)

Figure 4: Diverse applications of AutoMorFi. (A) Comparative morphometric analysis of glial cells from different models. Representative widefield fluorescence and brightfield images of glial cells from experimental models (*Drosophila* astrocyte-like glia, hiPSCs-derived microglia, human microglia, and mouse microglia) and their corresponding whole-cell outlines. UMAPs of 1,100 glial cells clustered based on 47 morphometric parameters or model system. **(B) Single object morphometric analysis.** Representative widefield fluorescence images of MAP2-immunolabeled primary neurons (white) from Ube3a 2x transgenic and wildtype mice and their corresponding whole-cell and skeletonized traces with an example of an added pseudo-object (white arrowhead). Six of 33 morphometric parameters were significantly different between genotypes in unpaired t-tests: whole cell perimeter (p=0.0138), whole cell height (p=0.0270), whole cell minimum feret (p=0.0116), whole cell convex area (p=0.0177), perimeter to area ratio, and solidity (p=0.0351). *N* = 14 per group. **(C) Acetylated-α-tubulin marker-specific morphometric and fluorescence intensity measurements.** Representative widefield fluorescence images of *Xenopus* MCCs indicated by centrin4-cfp (grey) with varying levels of ciliation indicated by acetylated-α-tubulin (red) and whole-cell outline of the marker (yellow). UMAPs of 508 MCCs based on 25 morphometric parameters after dimensionality reduction distributed across (1) 3 clusters determined by unsupervised kmeans clustering, (2) *Cp110* knockdown and rescue MCC phenotypes, and (3) marker fluorescence intensity. Histogram displays the relative proportion of the 3 clusters across phenotypes. **(D) Whole organism morphometric and NF-κB marker analyses.** Representative widefield fluorescence images of control and starved sea anemone polyps. DNA (blue), NF-κB (red), and AutoMorFi generated whole-object outline (yellow). Selected measurements are shown. Unpaired t-tests. *N* = 6 per group. **(E) Whole-image 2D morphometric analysis of photographed objects.** Representative image of corallites photographed under water and a corresponding whole-object outline and skeletonized trace. UMAPs of 628 corallites based on 21 morphometric parameters after dimensionality reduction distributed into clusters and lineages A–C. Histogram illustrates the proportion of the 3 clusters across lineages. Scale bars, 10 μm **(A-C)**; 100 μm **(D)**; 2 mm **(E)**.

Table 1 | List of 47 morphometric parameters.

Category	Parameter		Definition
Soma	1.	Soma area	Area of the object (μm^2)
	2.	Soma perimeter	Length of the outside boundary of the object (μm)
	3.	Soma width	Width of the smallest rectangle enclosing the object (μm)
	4.	Soma height	Height of the smallest rectangle enclosing the object (μm)
	5.	Soma major	Primary axis of the best fitting ellipse in the object (μm)
	6.	Soma minor	Secondary axis of the best fitting ellipse in the object (μm)
	7.	Soma circularity	Value of 1.0 indicates a perfect circle, 4π*area/perimeter^2
	8.	Soma feret	Maximum caliper, longest distance between any two points
	9.	Soma minimum feret	Minimum caliper diameter
	10.	Soma aspect ratio	Major axis / Minor axis
	11.	Soma roundness	Inverse of the aspect ratio, 4*area / (π*major axis^2)
	12.	Soma solidity	Area / Convex area
Whole cell	13.	Whole cell area	Area of the object (μm^2)
	14.	Whole cell perimeter	Length of the outside boundary of the object (μm)
	15.	Whole cell width	Width of the smallest rectangle enclosing the object (μm)
	16.	Whole cell height	Height of the smallest rectangle enclosing the object (μm)
	17.	Whole cell major (X)	Primary axis of the best fitting ellipse in the object (μm)
	18.	Whole cell minor (Y)	Secondary axis of the best fitting ellipse in the object (μm)
	19.	Whole cell circularity	Value of 1.0 indicates a perfect circle, 4π*area/perimeter^2
	20.	Whole cell feret	Maximum caliper, longest distance between any two points
	21.	Whole cell minimum feret	Minimum caliper diameter
	22.	Whole cell aspect ratio	Major axis / Minor axis
	23.	Whole cell roundness	Inverse of the aspect ratio, 4*area / (π*major axis^2)
	24.	Whole cell solidity	Area / Convex area
Skeletonized	25.	Total number of segments	Total number of slab segments
	26.	Number of junctions	Number of actual segment junctions
	27.	Number of end point voxels	Voxel with less than 2 neighbors
	28.	Number of junction voxels	Voxel with more than 2 neighbors
	29.	Number of slab voxels	Voxel with exactly 2 neighbors
	30.	Average branch length	Average length of branches (μm)
	31.	Number of triple points	Number of junctions with exactly 3 branches
	32.	Number of quadruple points	Number of junctions with exactly 4 branches
	33.	Maximum branch length	Maximum length of branches (μm)

Additional parameters	34.	Total branch length	Maximum branch length / Number of junction voxels
	35.	Cell spread	Whole cell aspect ratio / Number of end point voxels
	36.	Branch area ratio	Whole cell area / Soma area
	37.	Branch perimeter ratio	Whole cell perimeter / Soma perimeter
	38.	Whole cell convex area	Whole cell solidity / Whole cell area
	39.	Nodes	Number of end point voxels + Junction voxels + Slab voxels
	40.	Ramification index	Whole cell perimeter / Whole cell area)/2 x [√(πWhole cell area x XY)]
	41.	Perimeter to area ratio	Whole cell perimeter^2 / Whole cell area
	42.	Density	Whole cell area / (Whole cell major x Whole cell minor)
	43.	Process soma area ratio	Branch area / Soma area
	44.	Process whole cell area ratio	Branch area / Whole cell area
	45.	Skeleton to process ratio	Total branch length^2 / Branch area ratio
	46.	Branch points endpoints ratio	Number of slab voxels / Number of end point voxels
	47.	Whole cell solidity	Whole cell area / Whole cell convex area

Table 2 | Morphometric analysis of microglia in postmortem human MS and control brains.

Group	Patient ID	Area analyzed (μm^2)	[1]Mean NND ± s.e.m. (μm)
Control WM	Control_1 (45M)[2], Control_2 (59M)	320,000	41.69 ± 2.48
MS NAWM	MS_1 (68M), MS_2 (30M)	320,000	36.41 ± 1.93
MS Center	MS_1 (68M), MS_2 (30M)	320,000	38.62 ± 4.37
MS Rim	MS_1 (68M), MS_2 (30M)	320,000	27.42 ± 1.87

[1]Mean nearest neighbor distance (NND) of IBA-1$^+$ microglial cells, [2]Patient age in years and sex (M = male) in parentheses.

SUPPLEMENTARY INFORMATION 1

Prerequisites to running AutoMorFi.

Step I: Download and add the following plugins to the “plugins” folder of your ImageJ:

- “Excel.macro.extensions-3.3.2-jar-with-dependencies.jar”
- “script-editor-0.7.4-SNAPSHOT.jar”

To find the “plugins” folder on Mac:

- Go to Finder > Desktop > Search: “Fiji”
- Right-click on the Fiji logo > “Show package contents”
- Open the “plugins” folder
- Copy-and-paste the downloaded plugins

Windows

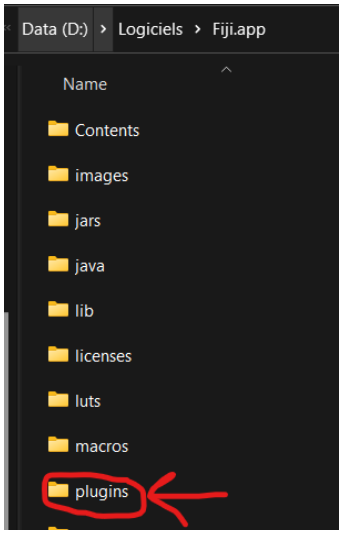

Mac

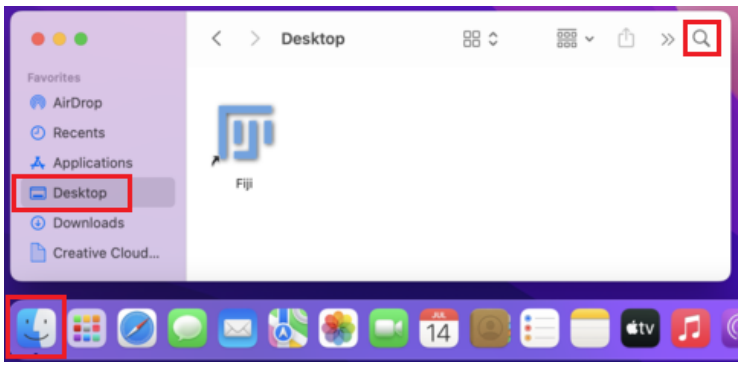

Step II: Update ImageJ/Fiji

- Start ImageJ/Fiji and select Help > Update… > Manage update site
- Select: ☑Excel Functions ☑Neuroanatomy
- Unselect: ☐ResultToExcel
- Close the “Manage update sites” window
- Close the “ImageJ Updater” window
- Restart ImageJ/Fiji

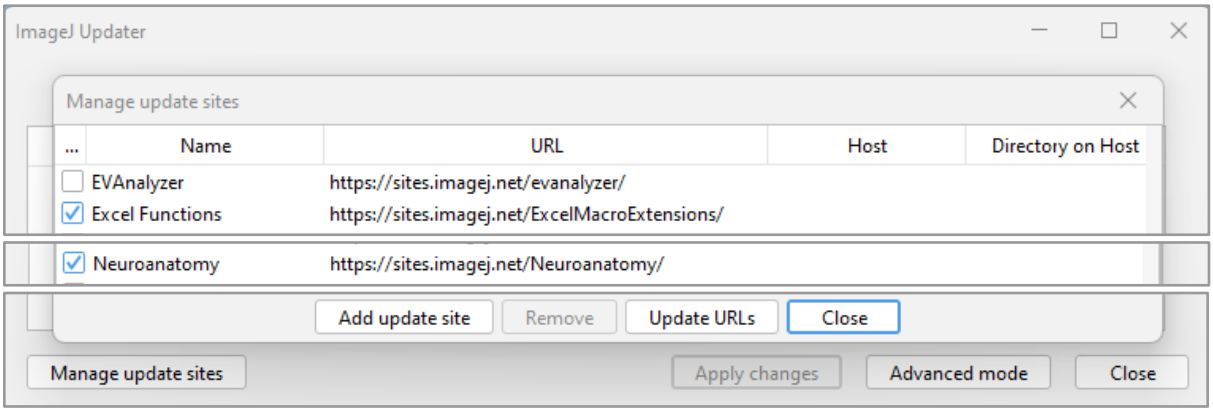

Step III: Range of measurements

1. Ensure your version of Fiji/ImageJ is updated before each analysis.
2. Set your Fiji/ImageJ as follows:
    - Analyze > Set measurements
    - Select the top 18 criteria
    - Click “OK”

Window

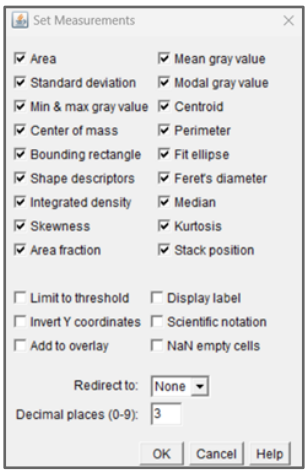

Mac

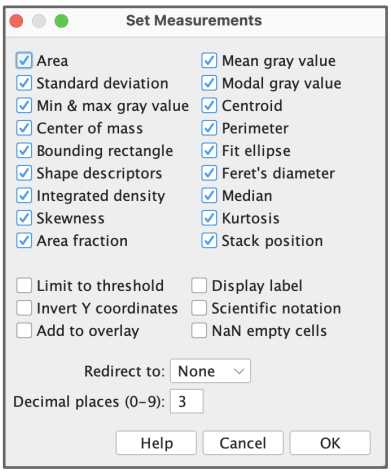

3. AutoMorFi requires the user to enter the size range of the cell soma and whole cell areas. To get these values:
    - Drag and drop the image you want to analyze onto Fiji/ImageJ
    - Make sure to work with a single-channel .tif image that is 8-bit and scaled.
    - Use the ‘straight’ tool to measure the diameter (in microns) of 5–10 cell somas and whole cells representing the average, smallest, and largest objects in the image.
    - With these diameter measurements, estimate the size ranges needed in the Analyze Particles wizard embedded within AutoMorFi. For example, if the soma diameters measured are 6.74, 7.56, 8.43, 13.74, and 12.33, the lower threshold value would be obtained as 6.74^2 = 45.43 and the upper threshold value would be obtained as 13.74^2 = 188.79. The range entered in the wizard could be 42-200.
    - Optimization tip: the ranges of soma and whole cell areas depend on the type of image and objects you are working with (e.g., cell type, cell density, method of image acquisition, etc.). After the first run, evaluate the accuracy of your soma and whole cell ranges by looking at the soma (SomaOutlines.tiff) and whole cell (WholeCellOutlines.tiff) outlines in your output folder.
        - too many nonspecific objects identified –> increase lower threshold value
        - small objects not captured –> decrease the lower threshold value
        - big objects not captured –> increase the upper threshold value

Windows

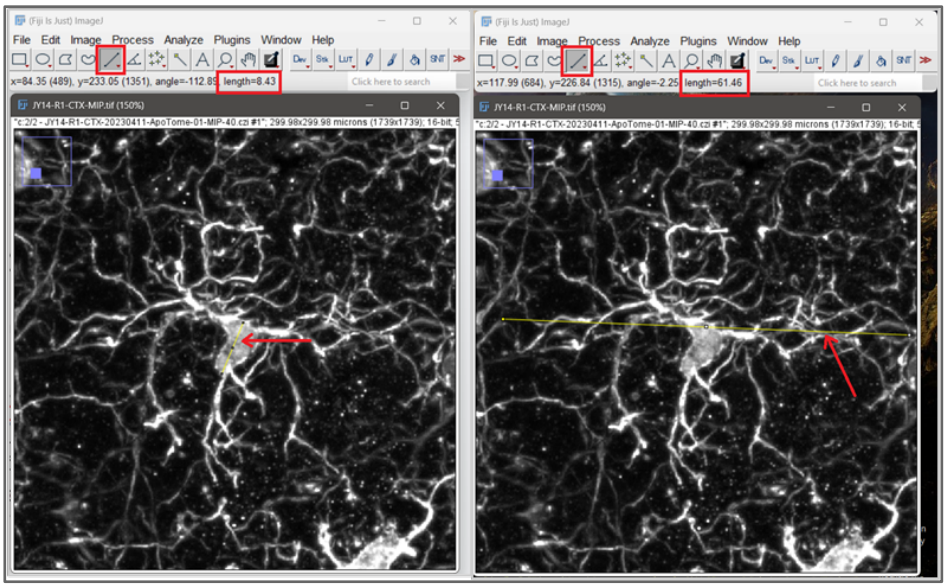
(Fiji Is Just) ImageJ
File Edit Image Process Analyze Plugins Window Help
x=84.35 (489), y=233.05 (1351), angle=-112.85 length=8.43
Click here to search
JY14-R1-CTX-MIP.tif (150%)
(Fiji Is Just) ImageJ
File Edit Image Process Analyze Plugins Window Help
x=117.99 (684), y=226.84 (1315), angle=-2.25 length=61.46
Click here to search
JY14-R1-CTX-MIP.tif (150%)

Mac

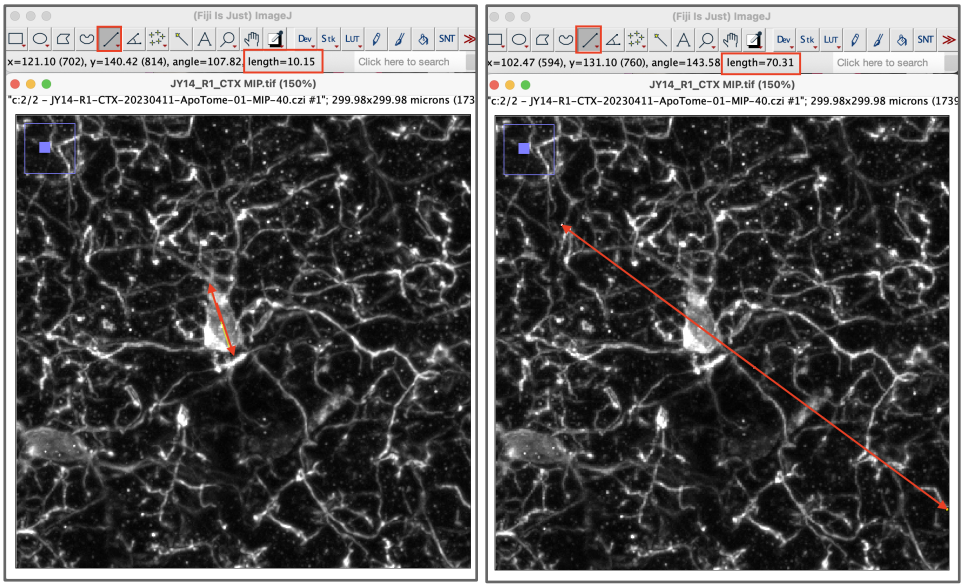
(Fiji Is Just) ImageJ
x=121.10 (702), y=140.42 (814), angle=107.82 length=10.15
Click here to search
JY14_R1_CTX MIP.tif (150%)
"c:2/2 – JY14-R1-CTX-20230411-ApoTome-01-MIP-40.czi #1"; 299.98x299.98 microns (173
(Fiji Is Just) ImageJ
x=102.47 (594), y=131.10 (760), angle=143.58 length=70.31
Click here to search
JY14_R1_CTX MIP.tif (150%)
"c:2/2 – JY14-R1-CTX-20230411-ApoTome-01-MIP-40.czi #1"; 299.98x299.98 microns (1739

SUPPLEMENTARY INFORMATION 2

Running the AutoMorFi macro

AutoMorFi works only on **single-channel 8-bit TIFF** images. Make sure the folder path leading to your image contains **no space, slash, or other special characters**. Use only letters, numerals, underscore, and dash.

Close any window that is open on Fiji/ImageJ. To start the AutoMorFi macro (AutoMorFi_3.ijm):

1. drag and drop the macro file in Fiji/ImageJ > press [Run]
2. select your image ("xxx.tif") > Click "Open"

Step 1: object identification by thresholding

On your screen, the original image (named "Temp") and the "Skeleton" image are displayed.

In the "Threshold" window, adjust the threshold of the "Skeleton" image:

1. select the "Skeleton" image (an error message will result if a different image is selected)
2. adjust the auto threshold method (ex: Default)
   Tip: set the display method to "Red" (instead of B&W) in the "Threshold" window
3. adjust the threshold using the first sliding bar
4. **click "Apply"** in the "Threshold" window
5. click "OK" to continue the analysis

Windows

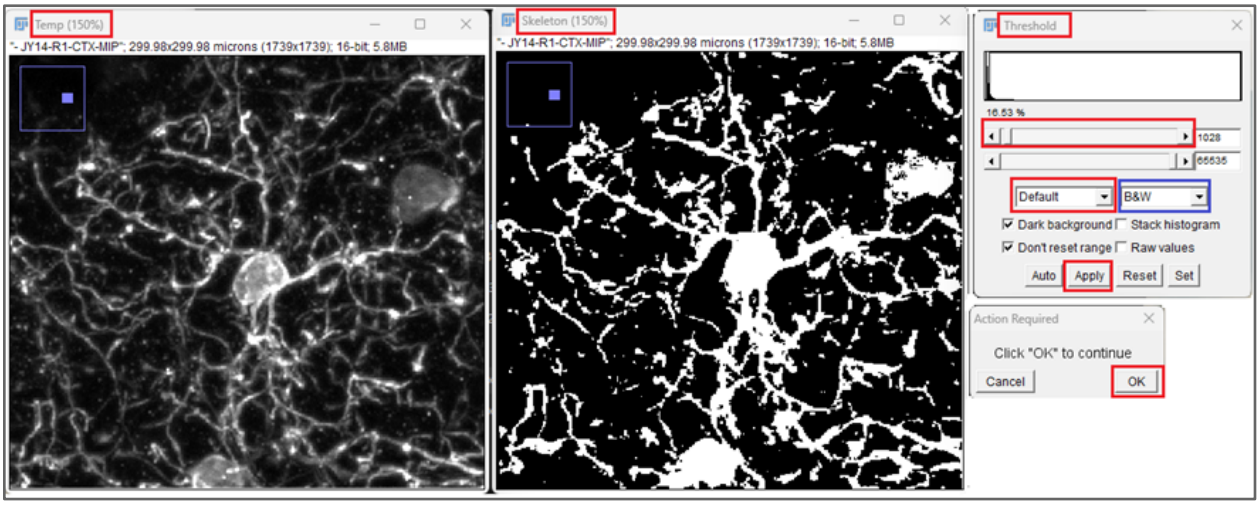

Mac

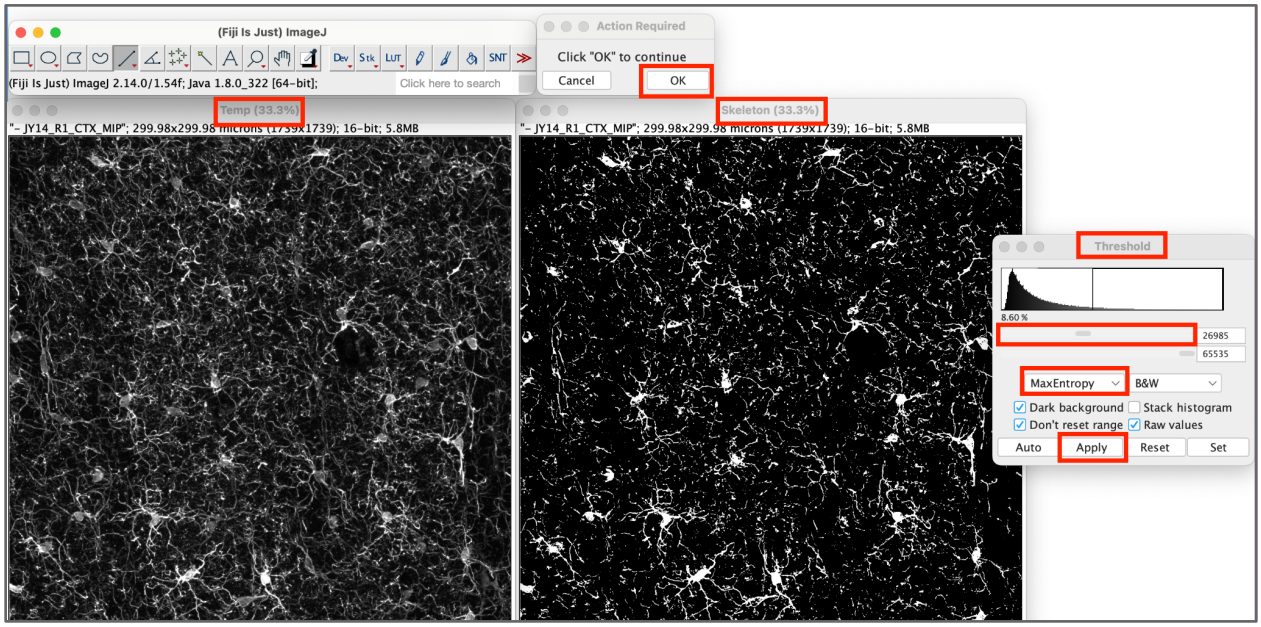

Step 2: connect disrupted processes using dilation (for objects with branches)

- Dilate Option window: if your cells are not branched, select “No” > click OK
- Dilate Option window: to connect disrupted processes, select “Yes” > click “OK”
- to **finish** the dilation: select “Finished” > “OK”
- to **revert** the dilation: select “Revert” > “OK” (only one dilation can be reversed)
- to **continue** dilating: select “Continue” > “OK” > “Yes” > “OK”

Windows

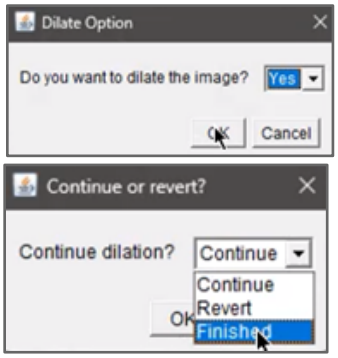

Mac

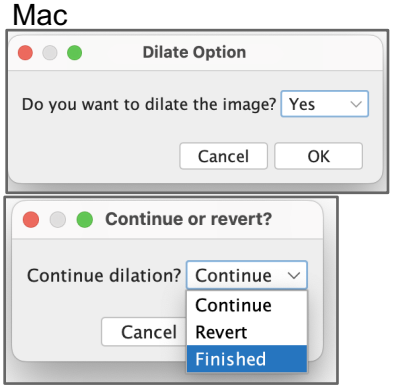

Step 3: object detection by diameter ranges

1. The **first** Analyze Particles window will analyze your cell **soma**
   - In “Size (micron)^2”, enter the calculated soma size range
   - Show: Masks, ☑ Display results, ☑ Add to manager, ☑ Overlay > “OK”
2. The **second** Analyze particles window will analyze your **whole cell**
   - In “Size (micron^2)”, enter the calculated whole cell size range
   - Show: Masks, ☑ Display results, ☑ Add to manager, ☑ Overlay > “OK”

Windows

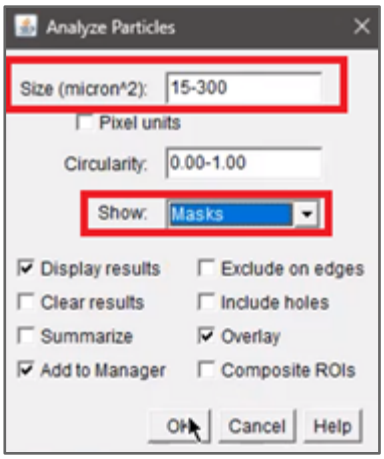

Mac

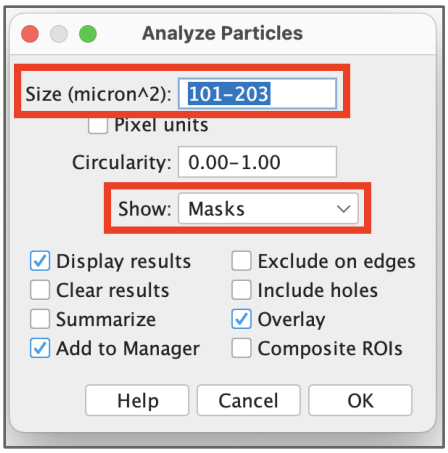

Step 4: deletion of false positive objects in the ROI manager

1. Select the objects by their number in the ROI manager (click on “Labels” if the numbers are not visible)
2. Click “Delete”
3. When you are done, click “Update” > “Deselect”
4. Click “OK” in the “ROI Deletion” window

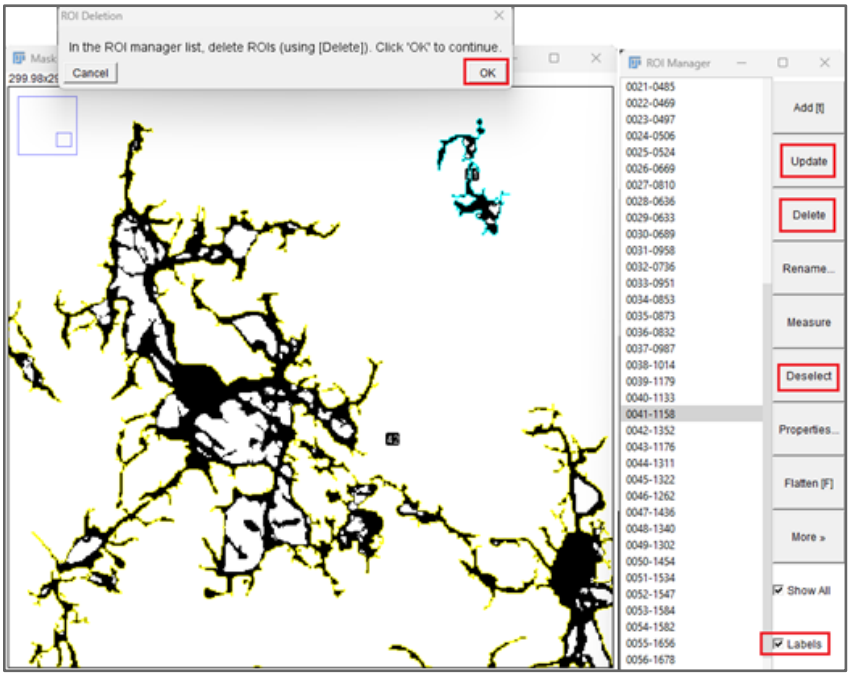

Let the macro run until the “Finish” window appears.

SUPPLEMENTARY INFORMATION 3

Troubleshooting for AutoMorFi

Error 1. Macro does not start
The image format, name, or image path is incorrect.
Solution 1: AutoMorFi only works on one-channel 8-bit TIFF images.
Solution 2: Make sure the folder path leading to your image contains no space, slash or special characters. Use only underscore or dash.

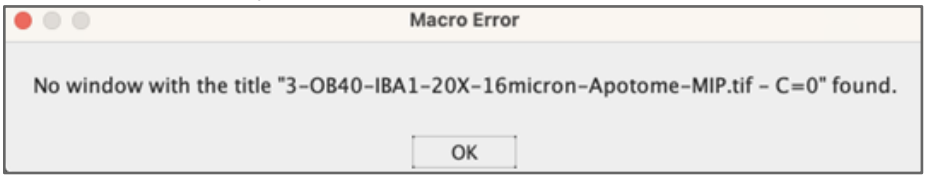

Error 2. Macro does not continue after step 1
A different image than “Skeleton” was selected and thresholded during step 2, or the user did not click “Apply” in the Threshold window before clicking “OK” in the Action Required window.
Solution: Make sure to adjust the threshold of the “Skeleton” image in the Threshold window.

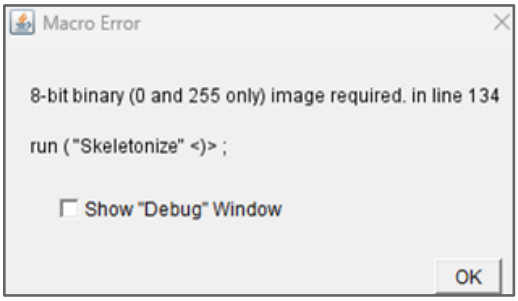

Error 3. Only one row of data is shown in the BranchInformation.csv and SkeletonResult.csv output files
The user did not click “Update” followed by “Deselect” in the ROI Manager window before clicking “OK” during **step 4 (deletion of false positive objects in the ROI manager).**

Error 4. Unresponsive macro or to interrupt the current run
Solution: Click “Kill”, at the bottom of the macro window.

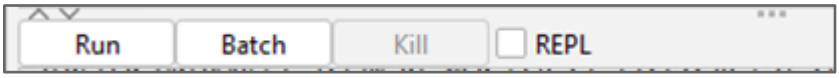

Error 5. “Default” thresholding incorrectly detects “soma” of the objects
AutoMorFi has a built-in automatic thresholding function for “soma” identification instead of the manual thresholding for whole-cell object identification in step 1 (i.e., object identification by thresholding). This can lead to incorrect “soma” identification in the SomaOutline.tif output.
Solution: Choose the appropriate AutoThreshold method to use before running AutoMorFi:

- Open your image on ImageJ/Fiji to identify the optimal AutoThreshold method

- Select: Image > Adjust > AutoThreshold (https://imagej.net/plugins/auto-threshold)
- In the AutoMorFi macro window, replace “Default” with the optimal AutoThreshold method (case sensitive) in line 68.
- Run AutoMorFi as usual.

```
68  setAutoThreshold("Default");
```

Error 6. Macro does not generate output from image containing only one object

AutoMorFi requires a minimum of 2 objects per image to run.

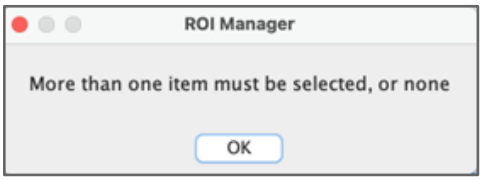

Solution: Create a second object in the ROI manager during step 4:

- In the ROI manager, click “More” > “Draw”
- Draw a rectangle in the background of the image (i.e., not on the object of interest)
- When you are done, click “Update” > “Deselect”
- Click “OK” in the “ROI Deletion” window

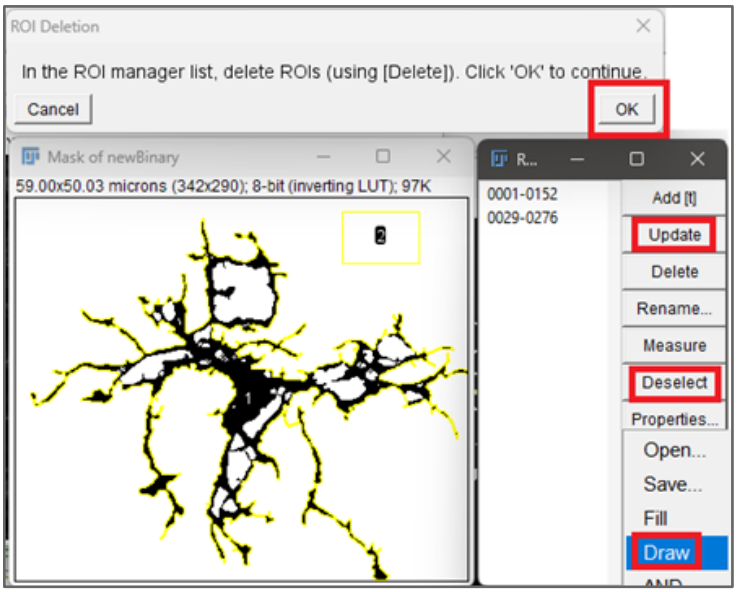

CODE FOR AUTOMORFI MACRO (IMAGEJ/FIJI-COMPATIBLE)

```
//AutoMorFi_3 macro

// clean up: makes sure no data is stored from previous macro use
// close all images
close("*");
// empty the ROI manager
roiManager("reset");
// empty the results table
run("Clear Results");
// configure that binary image are black in background, objects are white
setOption("BlackBackground", true);



//Obtain Image Path, Folder Path
path = File.openDialog("Choose a File");
basename = File.nameWithoutExtension();
dirname = File.getParent(path);
folder = dirname + File.separator + basename;


//Create Result Folders
if (File.exists(folder)) {
   print("Directory already exists, override the existing directory");
   list = getFileList(folder);
   for (i = 0; i < list.length; i++) {
         File.delete(folder + File.separator + list[i]); // Delete each file
         }
}
else {
   File.makeDirectory(folder);
}


//Open Image thru Bio-Format Importer
run("Bio-Formats Importer", "open="+path);
imageOriginPath = folder + File.separator + basename;
saveAs("tiff", imageOriginPath);

//Get Image size, Set scales
getPixelSize(unit, pixelWidth, pixelHeight);
scale = 1 / pixelWidth;
```

```
nameOrigin = getTitle();
microWidth = getWidth() / scale;
microHeight = getHeight() / scale;

//All Output Directories
binaryPath = folder + File.separator + "Binary";
somaResultsPath = folder + File.separator + "SomaResults.csv";
somaOutlinesPath = folder + File.separator + "SomaOutlines";
wholeCellResultsPath = folder + File.separator + "WholeCellResults.csv";
wholeCellOutlinesPath = folder + File.separator + "WholeCellOutlines";
skeletonPath = folder + File.separator + "Skeleton";
skeletonResultsPath = folder + File.separator + "SkeletonResults.csv";
branchInformationPath = folder + File.separator + "BranchInformation.csv";


//Duplicate original input twice. One for skeleton, the other for threshold reference.
run("Duplicate...", " ");
rename("Skeleton");
run("Duplicate...", " ");
rename("Temp");


//Process Binary Image
selectWindow(basename+".tif");
run("Enhance Contrast", "saturated=0.35");
run("Apply LUT");
run("8-bit");
setAutoThreshold("Default");
run("Convert to Mask");
run("Invert LUT");
run("Make Binary");
run("Despeckle");
rename("Binary");


//Process Skeleton, Manually set threshold
selectWindow("Skeleton");
run("Threshold...");//https://imagej.net/plugins/auto-threshold#available-methods
waitForUser;   //User adjust threshold here
close("Threshold");
close("Temp");

//Dilation Dialogs
selectWindow("Skeleton");
```

```
stack_count = 0; //Keep track of the number of dilations
rename("Mask_" + stack_count);
while (true) {
   //Creating dialog with dilate option "Yes"/"No"
   Dialog.create("Dilate Option");
   Dialog.addChoice("Do you want to dilate the image?", newArray("Yes", "No"));
   Dialog.show();
   choice = Dialog.getChoice();

   //When choosing "Yes", dilate the image from the previous stack
   if (choice == "Yes") {
      selectWindow("Mask_" + stack_count);
      run("Duplicate...", "title=Temp");
      run("Dilate");
      stack_count++;
      selectWindow("Temp");
      rename("Mask_" + stack_count);

      //Creating dialog with options "Continue", "Revert", "Exit"
      Dialog.create("Continue or revert?");
      Dialog.addChoice("Continue dilation?", newArray("Continue", "Revert", "Finished"));
      Dialog.show();
      secondChoice = Dialog.getChoice();
      //When Continue, enter the next iteration
      //When Revert, return to the previous iteration
      //When Exit, save the current iteration and process to skeletonization
      if (secondChoice == "Continue") {
                              close("Temp");
      } else if (secondChoice == "Revert") {
         close("Temp");
         close("Mask_" + stack_count);
         stack_count--;
      } else {
         close("Temp");
         break;
      }
   } else {
         break;
   }
}
for (i = 0; i < stack_count; i++) {
         close("Mask_" + i);
}
selectWindow("Mask_" + stack_count);
```

```
//Dilation Dialog ends


//Create skeleton, overlay with Binary using imageCalculator
rename("Skeleton");
run("Skeletonize");
imageCalculator("add create", "Binary", "Skeleton");
close("Skeleton");
close("Binary");
selectWindow("Result of Binary");
rename("newBinary");
saveAs("tiff", binaryPath);
rename("newBinary");


//Soma Analysis
selectWindow("newBinary");
run("Duplicate...", " ");
rename("newBinary2");
run("Watershed");
run("Clear Results");
run("Analyze Particles...");
n = roiManager("count");
somaArray = newArray(n);
for (var i = 0; i < n; i++) {
   somaArray[i] = i;
}
selectWindow("Results");
saveAs("Measurements", somaResultsPath);
run("Clear Results");
selectWindow("newBinary2");
open(imageOriginPath+".tif");
run("Enhance Contrast", "saturated=0.35");
run("Apply LUT");
roiManager("Select", somaArray);
selectWindow(basename+".tif");
setOption("Show All", true);
run("Flatten");
saveAs("tiff",somaOutlinesPath);
run("Close");
close("newBinary2");
roiManager("reset");

//Cell Analysis
```

```
selectWindow("newBinary");
run("Analyze Particles...");
n1 = roiManager("count");
// Can delete ROIs here
waitForUser("ROI Deletion", "In the ROI manager list, delete ROIs (using [Delete]). Click 'OK' to
continue.");
n2 = roiManager("count");
if (n2 < n1) {
        run("Clear Results");
        roiManager("multi-measure append");
}
cellArray = newArray(n2);

for (var i = 0; i < n2; i++) {
   cellArray[i] = i;
}
open(imageOriginPath+".tif");
run("Enhance Contrast", "saturated=0.35");
run("Apply LUT");
roiManager("Select", cellArray);
selectWindow(basename+".tif");
setOption("Show All", true);
run("Flatten");
saveAs("tiff",wholeCellOutlinesPath);
roiManager("XOR");
run("Create Mask");
selectWindow("Results");
saveAs("Measurements", wholeCellResultsPath);
close("newBinary");
run("Clear Results");
close("newBinary");


//Skeletonize and Analyze Skeletons
selectWindow("Mask");
rename("Skeleton");
run("Skeletonize");
saveAs("tiff",skeletonPath);
rename("Skeleton");
run("Analyze Skeleton (2D/3D)","prune=[lowest intensity branch] show display");
selectWindow("Results");
saveAs("Measurements", skeletonResultsPath);
selectWindow("Branch information");
saveAs("Measurements", branchInformationPath);
```

```
//Close all windows, end macro.
close("*");
selectWindow("ROI Manager");
run("Close");
selectWindow("Results");
run("Close");
if (isOpen("BranchInformation.csv")) {
	selectWindow("BranchInformation.csv");
	run("Close");
}

waitForUser("Finish", "Results in the output folder. Click 'OK' to exit.");
```